INTERNATIONAL JOURNAL FOR NUMERICAL METHODS IN ENGINEERING
Int. J. Numer. Meth. Engng 2000; **49**:1191–1209

An implicit finite element material model for energetic particulate composite materials

Robert M. Hackett[‡] and Joel G. Bennett[*,†,§]

Los Alamos National Laboratory, ESA-EA, MS P946, Box 1663, Los Alamos, NM 87544, U.S.A.

SUMMARY

The predisposition of energetic particulate composite materials, or high explosives (HE), to ignition by bulk heating (cookoff) poses serious safety problems. Because unexpected initiation of HE must be a major consideration in any activity involving employment of the material, its behaviour under a variety of conditions is of much interest. The formulation of a numerical constitutive model that can be employed in an implicit finite element code to predict the mechanical and ignition behaviour of HE is presented. The capability of the developed material model is then demonstrated through its implementation in the ABAQUS finite element code to simulate the response of HE test configurations. The simulated response is found to compare favourably with the physical test results, in the cases where test data exist. Copyright © 2000 John Wiley & Sons, Ltd.

KEY WORDS: high explosives; finite element constitutive model; mechanical behaviour; non-shock ignition

1. INTRODUCTION

An understanding of the non-shock ignition response of energetic particulate composite materials is extremely important relative to safety assessments of the handling of these material systems. This subject has received attention since the discovery in the early l980s that mild mechanical shocks to solid propellant motors could lead to explosions having a violence approaching that of those produced by strong shock waves in the process known as shock to detonation transition (SDT) [1, 2]. The term non-shock ignition is used since the explosions are caused by mild multi-dimensional mechanical shocks. Until recently, the investigation of these phenomena has focused on experimental determinations of 'go/no go' conditions for ignition associated with impact velocity conditions, with limited effort directed toward identifying the underlying complex micromechanisms the interactions of which cause ignition to occur. Most experiments have been limited, at best, to observing the exterior of the charge and to making measurements of the bulk response, such as time to explosion, violence of event, and, in some cases, location of the point of ignition [3]. The

[*]Correspondence to: Joel G. Bennett, Los Alamos National Laboratory, ESA-EA, MS P946, Box 1663, Los Alamos, NM 87544, U.S.A.
[†]E-mail: jbennett@lanl.gov
[‡]Professor Emeritus of Civil Engineering, University of Mississippi, Oxford, MS, U.S.A.
[§]Technical Staff Member, Los Alamos National Laboratory, Los Alamos, NM, U.S.A.

Received 2 July 1999
Revised 8 February 2000

internal behaviour of the charge being hidden from view, sparse data are available for making comparisons with computational model predictions.

The importance of the development of such computational models, having the capability of accurate and efficient predictions, goes without saying since it can ultimately achieve the goal of replacing expensive experimental testing. Additionally, it has been abundantly demonstrated that numerical modelling can provide insight into material behaviour that cannot be acquired through experimental testing. A major motivation for having an *implicit* finite element computer code material model for HE is to be able to simulate the slow heating of the material with resulting chemical decomposition, the thermal strain and confined pre-stress effects, followed by a large pressure transient (a sequence that needs to be examined for safety and surety in the transportation of HE materials). A set of experiments on this subject are in progress at the Los Alamos National Laboratory (LANL) that are referred to by name as mechanically coupled cookoff and they are described in more detail in the 'future applications' section of this paper.

Although there are several micromechanical processes that may be responsible, it is generally agreed that non-shock ignition occurs because of an isolated high-temperature region in the material that is referred to as a 'hot-spot'. It is also generally felt that these regions are caused by the interaction of stress or shock waves with defects in the material, and that the formation of the hot-spot is strongly related to the chemical, mechanical and thermal properties of the material; however, the dominant micromechanisms and interactions have not been generally agreed upon. Some of the micromechanisms which have been suggested and investigated are viscous heating, localized plastic work, friction between grains, hydrodynamic void (pore) collapse with adiabatic heating of the entrapped gas, internal shear, and shock interaction at density discontinuities [1–6]. It is likely that all of these can produce a hot-spot under certain circumstances; however, Dienes [7] has carried out an order-of-magnitude analysis that indicates that the mechanism having the greatest potential for heat generation is friction on shear crack surfaces. Shear cracking certainly occurs in these materials, it having been observed in experiments conducted by Howe [8] and others, although the cracks are difficult to detect. Dienes [9] has also demonstrated that the inclusion of the effect of frictional heating within the context of his statistical crack mechanics (SCRAM) model can induce ignition. Bennett *et al*. [10], developed the constitutive model and the underlying formulation for the characterization of an energetic particulate composite material, the plastic (polymeric) bonded explosive PBX 9501, for an explicit finite element code. Their model has been employed successfully in some of the non-shock analyses carried out at LANL. The work reported in that reference had the same basic mechanical model that is developed in this paper, but an explicit code requires only a stable time step and an update of the stress of the material model. In this paper the equations are manipulated differently to develop the tangent stiffness matrix that is required for a conventional implicit version of the model, and new features are added. The totally new features include: (1) the addition of a tensile-cracking damage criterion, (2) the equations governing the contribution of all inelastic work rates and bulk material chemical kinetics to the *bulk* material temperature rise which is then used as the conduction temperature boundary condition for the hotspot model. In the explicit model, hotspot conduction was into the ambient temperature, because it was assumed that the response time scales were such that bulk material thermal response would not occur during the period of interest. Later experimental work demonstrated that this assumption was not always true and that bulk material thermal response should be included.

The insight provided by Dienes [9] is heavily relied upon in the model formulation to be presented. The goal is that of developing a viscoelastic, isotropic modified SCRAM model with ignition for implementation in an implicit finite element code which can be employed in

accurately and efficiently simulating the three-dimensional mechanical response, including the non-shock ignition, of HE.

2. MODEL FORMULATION

The time dependence of fracture has been explored fairly extensively for a number of different types of materials. For example, Bazant and Li [11] and Li and Bazant [12], have demonstrated through a compliance formulation and numerical implementation, respectively, that for concrete process can be considered as having two sources, the viscoelasticity of material behaviour in the bulk of the structure and the rate process of the breakage of bonds in the fracture zone which causes the softening law for crack opening to be rate-dependent. The formulation presented here is based primarily upon the work of Addessio and Johnson [13] and combines a generalized Maxwell (viscoelasticity) model with the SCRAM approach of Dienes [9]. The SCRAM model is a physically based micromechanical approach to the large deformation and cracking of brittle materials. During deformation, the distribution of the cracks is assumed to remain random and the initial distribution of the cracks exponential.

Using Cartesian tensor index notation, the strain is given by the kinematic relationship

$$\varepsilon_{ij} = \tfrac{1}{2}(u_{j,i} + u_{i,j}), \quad i,j = 1,2,3 \tag{1}$$

where the u_i are the material deformation variables. It can be decomposed into deviatoric and mean components

$$\varepsilon_{ij} = e_{ij} + \varepsilon_{\mathrm{m}}\delta_{ij} \tag{2}$$

where δ_{ij} is the Kronecker delta, where the mean strain is defined by

$$\varepsilon_{\mathrm{m}} = \tfrac{1}{3}\varepsilon_{ii} \tag{3}$$

The stress can likewise be decomposed into deviatoric and mean components

$$\sigma_{ij} = s_{ij} + \sigma_{\mathrm{m}}\delta_{ij} \tag{4}$$

where the mean stress is defined by

$$\sigma_{\mathrm{m}} = \tfrac{1}{3}\sigma_{ii} \tag{5}$$

and is related to the mean strain through the expression

$$\sigma_{\mathrm{m}} = 3K\varepsilon_{\mathrm{m}} \tag{6}$$

where K is the bulk modulus of the material.

In a deviatoric Maxwell model, a single spring and dashpot in series, the relationship between stress and elastic strain is

$$s_{ij} = 2Ge^{\mathrm{e}}_{ij} \tag{7}$$

where G is the shear modulus, and the relationship between stress and viscous strain rate is

$$s_{ij} = 2\eta\dot{e}^{\mathrm{v}}_{ij} \tag{8}$$

where η is the viscosity of the dashpot and where the dot over the variable indicates the time rate of change of the variable. Taking the partial derivative of Equation (7) and combining the result with Equation (8), i.e. adding viscous and elastic strain rates, gives

$$\dot{s}_{ij} = 2G\dot{e}_{ij}^{\mathrm{ve}} - \frac{s_{ij}}{\tau} \tag{9}$$

where the relaxation time τ is given by

$$\tau = \frac{\eta}{G} \tag{10}$$

For the viscoelastic solid, *represented by a generalized deviatoric Maxwell model*, with the strain being common for all elements of the model and the stresses for the individual elements being additive, i.e.

$$s_{ij} = \sum_{n=1}^{N} s_{ij}^{(n)} \tag{11}$$

where N is the number of elements in the generalized Maxwell model and $s_{ij}^{(n)}$ is the deviatoric stress component for the nth element, the relationship between the deviatoric stress rate and the viscoelastic deviatoric strain rate and deviatoric stress, referring to Equation (9), is given by

$$\dot{s}_{ij} = \sum_{n=1}^{N} \left(2G^{(n)}\dot{e}_{ij}^{\mathrm{ve}} - \frac{s_{ij}^{(n)}}{\tau^{(n)}} \right) \tag{12}$$

where $G^{(n)}$ and $\tau^{(n)}$ are the shear modulus and relaxation time, respectively, for the nth Maxwell element.

The cracking deviatoric strain versus deviatoric stress relationship [13] is

$$e_{ij}^{\mathrm{cr}} = \beta c^3 s_{ij} \tag{13}$$

where c is the average crack radius and β is a parameter that relates the shear modulus and the initial flaw size through the expression

$$\beta = \frac{1}{2Ga^3} \tag{14}$$

where a is the initial flaw size and

$$G = \sum_{n=1}^{N} G^{(n)} \tag{15}$$

Combining Equations (13) and (14) yields a relationship between the cracking deviatoric strain and the average crack radius

$$2Ge_{ij}^{\mathrm{cr}} = \left(\frac{c}{a} \right)^3 s_{ij} \tag{16}$$

Taking the partial derivative of Equation (16) with respect to time gives the expression

$$2G\dot{e}_{ij}^{\mathrm{cr}} = 3\left(\frac{c}{a} \right)^2 \frac{\dot{c}}{a} s_{ij} + \left(\frac{c}{a} \right)^3 \dot{s}_{ij} \tag{17}$$

The total deviatoric strain, the sum of the viscoelastic deviatoric strain and the cracking deviatoric strain, is given by

$$e_{ij} = e_{ij}^{\mathrm{ve}} + e_{ij}^{\mathrm{cr}} \tag{18}$$

Combining Equations (12), (17) and (18) gives an expression for the deviatoric stress in terms of combined viscoelastic and microcracking response:

$$\dot{s}_{ij} = \psi \dot{e}_{ij} - \theta(s_{ij} + \lambda_{ij}) \tag{19}$$

where

$$\psi = \frac{2G}{1 + (c/a)^3} \tag{20}$$

$$\theta = \frac{3(c/a)^2 \dot{c}/a}{1 + (c/a)^3} \tag{21}$$

and

$$\lambda_{ij} = \frac{\sum_{n=1}^{N} s_{ij}^{(n)}/\tau^{(n)}}{3(c/a)^2 \dot{c}/a} \tag{22}$$

The expression for the deviatoric stress rate for the nth Maxwell element is given by

$$\dot{s}_{ij}^{(n)} = 2G^{(n)} \dot{e}_{ij} - \frac{s_{ij}^{(n)}}{\tau^{(n)}} - \frac{G}{G^{(n)}} \left[3 \left(\frac{c}{a} \right)^2 \frac{\dot{c}}{a} s_{ij} + \left(\frac{c}{a} \right)^3 \dot{s}_{ij} \right] \tag{23}$$

An evolution equation defining crack growth rate is required. Consistent with the observations and conclusions of Dienes [9], it is assumed that the growth rate of the average crack radius is functionally dependent upon the stress intensity. The equations below are from Dienes [14] and Dienes and Kershner [15], with modifications for tension and friction provided by Johnson [16]. The cracking rate is either

$$\dot{c} = v_{\max} \left(\frac{K_I}{K'} \right)^m, \quad K_I < K' \tag{24}$$

or

$$\dot{c} = v_{\max} \left[1 - \left(\frac{K_{0\mu}}{K_1} \right)^2 \right], \quad K_I \geqslant K' \tag{25}$$

where

$$K_I = \left(\frac{3\pi c}{2} s_{ij} s_{ij} \right)^{1/2}, \quad \sigma_{\mathrm{m}} < 0 \tag{26}$$

or

$$K_I = \left(\frac{3\pi c}{2} \sigma_{ij} \sigma_{ij} \right)^{1/2}, \quad \sigma_{\mathrm{m}} \geqslant 0 \tag{27}$$

and

$$K' = K_{0\mu}\left(1 + \frac{2}{m}\right)^{1/2} \tag{28}$$

$$K_1 = K'\left(1 + \frac{m}{2}\right)^{1/m} \tag{29}$$

$$K_{0\mu} = K_0\left[1 - \frac{\pi\mu'\sigma_{\mathrm{m}}c^{1/2}}{K_0}\left(1 - \frac{\mu'\sigma_{\mathrm{m}}c^{1/2}}{K_0}\right)\right]^{1/2} \tag{30}$$

$$\mu' = \left[\frac{45}{2(3 - 2\mu_{\mathrm{s}}^2)}\right]\mu_{\mathrm{s}} \tag{31}$$

where $v_{\max}$ is the maximum value of the rate of growth of the average crack radius, K_0 is the threshold value of stress intensity, m is a cracking parameter and μ_{s} is the static coefficient of friction.

In the explicit finite element model of Bennett *et al.* [10], a thermal hot-spot ignition model is described. That model is used to compute the 'runaway' temperature history observed in the non-shock HE ignition experiments carried out on PBX 9501. However, in a review of those experiments, it has been concluded that the temperature field measurements taken during that activity represent bulk thermal field behaviour as well as hot-spot behaviour. Thus, in this model, equations to describe the bulk thermal behaviour on a continuum level have been implemented. Ignition is still determined as the runaway hot-spot temperature, but the hot-spot is assumed to conduct into the bulk temperature field that exists within an element.

The rate of change of the bulk material temperature is caused by a combination of dissipative and volumetric work rates and bulk material chemical heating. The dissipative mechanisms employed in this model include the inelastic work contributions from both viscous and cracking effects. Conduction can also contribute to the bulk thermal change. An energy balance on a differential volume of the bulk material gives

$$\dot{T} = \alpha T_{,ii} - \gamma T\dot{\varepsilon}_{jj} + \frac{\mathfrak{I}}{\rho C_{\mathrm{v}}}[(\dot{w})_{\mathrm{ve}} + (\dot{w})_{\mathrm{cr}}] + P_{\mathrm{he}}\dot{q}_{\mathrm{ch}} \tag{32}$$

The heating terms on the right-hand side of this equation are:

(1) the rate of conduction, with $\alpha = k/\rho C_{\mathrm{v}}$, the thermal diffusivity, being the thermal conductivity divided by the product of the density and the specific heat at constant volume,
(2) the adiabatic compression heating rate, with γ being the Gruneisen coefficient (~ 1 for PBX 9501),
(3) the inelastic work rates because of viscous effects, $(\dot{w})_{\mathrm{ve}}$, and cracking damage $(\dot{w})_{\mathrm{cr}}$, with $\mathfrak{I}$ being a conversion constant of these inelastic work rates to a heating rate,
(4) the bulk chemical heating, using the Arrhenius first-order chemical kinetics model described below in the hot-spot model, with P_{he} being the volume per cent of HE and $\dot{q}_{\mathrm{ch}}$ the chemical heating rate.

For the N-component Maxwell model, the viscous work rate is

$$(\dot{w})_{\mathrm{ve}} = \sum_{n=1}^{N} s_{ij}^{(n)} \dot{e}_{ij}^{\mathrm{ve}} = \sum_{n=1}^{N} \frac{s_{ij}^{(n)} s_{ij}^{(n)}}{2G^{(n)}\tau^{(n)}} \tag{33}$$

and the cracking damage work rate is

$$(\dot{w})_{\mathrm{cr}} = s_{ij}\dot{e}_{ij}^{\mathrm{cr}} = \frac{1}{2G}\left[3\left(\frac{c}{a}\right)^2 \frac{\dot{c}}{a} s_{ij}s_{ij} + \left(\frac{c}{a}\right)^3 s_{ij}\dot{s}_{ij}\right] \tag{34}$$

In Equation (32), $\mathfrak{I}$, the fractional multiplier of the amount of inelastic work that is converted to heat, is taken to be 95 per cent (a traditional assumption for metals). However, it can be noted in a recent report [17] of experimental measurements of this factor for some metals, that the value of 95 per cent is only achieved after some amount of inelastic strain has occurred. Presumably, some of the initial inelastic work goes into molecular rearrangement of the material. In the absence of data for these energetic materials, however, the traditional assumption is followed.

In non-shock ignition processes, the time and length scales for conduction in the continuum are generally very large compared to the time and length scales for the other heating mechanisms, a fact which can be verified by comparing the time constant for conduction (typical element cross-section/diffusivity) to the time constant for deformation (typical element length/dilatational wave speed). Thus, for bulk thermal changes in non-shock ignition, the bulk conduction in Equation (32) can be neglected. In cookoff modelling of accidents and experiments, bulk conduction for the 'cooking' period (slow heat-up), can be modelled separately from the mechanical response in the ignition phase. The temperature field in the mechanical model can be specified as an initial state to include the thermal strains. If the conduction term in Equation (32) is neglected, the adiabatic temperature change within an element can be computed and integrated in time as a state variable change at the element integration points. In the hot-spot model described below, the length scale is small enough that conduction must be included and the hot-spot is assumed to conduct into the bulk temperature field calculated from Equation (32).

The hot-spot model employed herein is the same model that is described in some detail in Reference [10] and is summarized in the following for completeness. In the SCRAM model [9], it is assumed that there is a statistical distribution of randomly oriented microcracks in the material. The hot-spot length scale is such that the crack appears infinite in extent relative to the size of the region of thermal influence. It is assumed that if the shear stress on a crack surface causes the static friction force on the surface to be exceeded, adjacent crack faces will slip, and heat will be generated. An energy balance for the crack model yields the modified [18] equations that govern one-dimensional heat transfer near the crack face:

$$\frac{\partial}{\partial y}\left(k_{\mathrm{f}}\frac{\partial T}{\partial y}\right) + \rho_{\mathrm{f}}\Delta H Z \mathrm{e}^{-E/RT} - \mu_{\mathrm{d}}\sigma_{\mathrm{m}}\frac{\partial v_x}{\partial y} = \rho_{\mathrm{f}}C_{\mathrm{f}}\dot{T}, \quad l_{\mathrm{f}} \geqslant y \geqslant 0 \tag{35}$$

and

$$\frac{\partial}{\partial y}\left(k_{\mathrm{s}}\frac{\partial T}{\partial y}\right) + \rho_{\mathrm{s}}\Delta H Z \mathrm{e}^{-E/RT} = \rho_{\mathrm{s}}C_{\mathrm{s}}\dot{T}, \quad y > l_{\mathrm{f}} \tag{36}$$

where T is the absolute temperature, k_i is the thermal conductivity, C_i is the heat capacity, μ_{d} is the dynamic coefficient of friction, $\partial v_x/\partial y$ is the gradient of particle velocity parallel to the crack face in a direction normal to the crack face, ρ_i is the mass density, ΔH is the heat of

detonation, Z is a pre-exponential factor, E is the Arrhenius activation energy, R is the universal gas constant and t is the time variable. Note that the hot-spot is viewed as a process zone of length l_f, quite possibly a fluid phase, in which friction and viscous effects caused by friction occur (thus, the subscript f), while the remaining portion of the region of hot-spot influence is a solid phase (thus, the subscript s). The hot-spot length l_f is to be determined (by simulation of non-shock ignition experiments for example); the frictional heat generation is volumetric, over the hot-spot volume. In Equations (35) and (36), the first term on the left-hand side represents the heat per unit volume conducted away from the hot-spot while the second term represents the Arrhenius first-order chemical kinetics expression for the heat generated per unit volume by the energetic component of the material; the right-hand side represents the heat per unit volume stored in the region of hot-spot influence. In addition, the model includes the latent heat absorbed or liberated during melt/resolidification, using the equivalent enthalpy method [19]. A microcrack is assumed to always exist normal to the direction of the maximum principal deformation rate in each element. The maximum principal deformation rate and its direction are determined within each element from the strain rate tensor. The deviatoric stress on a plane normal to this direction is computed and a check is made to determine whether the value exceeds that of the product of the static coefficient of friction and the compressive pressure (if the pressure is positive, the crack is assumed to be open, with no heat generated). If the maximum shear stress on this plane exceeds this value, the crack is assumed to slip, and heat is generated.

Equations (35) and (36) must be solved in each element at each time step. A weighted residual approach, which, in effect, is a one-dimensional finite element procedure, is used. The temperature is assumed to vary in the local co-ordinate as

$$T = H_1(\xi)T_1 + H_2(\xi)T_2 + H_3(\xi)\phi_1 + H_4(\xi)\phi_2 \tag{37}$$

where the T_i are the temperatures at the node i, the ϕ_i are the temperatures on the interior of the local domain and H_i are the interpolation functions. The geometry is assumed to map as

$$y = N_1 y_1 + N_2 y_2 \tag{38}$$

with the N_i being the standard linear interpolation functions. The chemical heat generation within the domain is also assumed to interpolate in this manner, i.e.

$$\dot{Q}_{\mathrm{ch}} = \sum_i \dot{Q}_{\mathrm{ch}_i} \tag{39}$$

With this formulation, the gradients of temperature within the region $-1 \leqslant \xi \leqslant 1$ can be resolved accurately since the interpolation functions for the temperatures, H_i, are cubic polynomials. The resulting matrix equations can be assembled into the form

$$\underline{\underline{k}}\,\underline{T} + \underline{\dot{Q}} = \underline{\underline{C}}\,\underline{\dot{T}} \tag{40}$$

which can be integrated in time. The hot-spot formulation can be assessed separately from the implementation into the implicit finite element code by driving the isolated hot-spot model with a pressure and a deviatoric deformation rate.

3. IMPLEMENTATION IN ABAQUS

Employing the constitutive model formulation presented, the equations for a user material (UMAT) subroutine for implementation in the implicit ABAQUS finite element code will be developed [20]. In order to incorporate the microcracking and thermal effects, a number of additional subroutines, called from UMAT, are necessary. These subroutines will be discussed later in this section. Combining Equations (4), (6) and (19) yields the expression

$$\theta\sigma_{ij} + \dot{\sigma}_{ij} = 3K(\theta\varepsilon_m + \dot{\varepsilon}_m) + \psi\dot{e}_{ij} - \theta\lambda_{ij} \tag{41}$$

Rearranging Equation (41) somewhat, yields the expression

$$\theta\sigma_{xx} + \dot{\sigma}_{xx} = \theta K\varepsilon_{\mathrm{v}} + \left(K - \frac{\psi}{3}\right)\dot{\varepsilon}_{\mathrm{v}} + \psi\dot{\varepsilon}_{xx} - \theta\lambda_{xx} \tag{42}$$

for the global x-direction on a plane $x = \text{constant}$, with similar expressions for the y- and z-direction, and

$$\theta\sigma_{xy} + \dot{\sigma}_{xy} = \frac{\psi}{2}\dot{\varepsilon}_{xy} - \theta\lambda_{xy} \tag{43}$$

for the x-direction on the plane $y = \text{constant}$, with similar expressions for the y- and z-direction, where

$$\varepsilon_{\mathrm{v}} = \varepsilon_{ii} \tag{44}$$

It should be noted that a factor of 2 is included in the denominator in Equation (43) because the ABAQUS code uses engineering strains instead of tensor strains.

Consistent with the ABAQUS UMAT formulation, the central difference operator is applied to Equations (42) and (43), yielding

$$\left(1 + \frac{\theta\Delta t}{2}\right)\Delta\sigma_{xx} = \left[K\left(1 + \frac{\theta\Delta t}{2}\right) - \frac{\psi}{3}\right]\Delta\varepsilon_{\mathrm{v}} + \psi\Delta\varepsilon_{xx} + \theta\Delta t(K\varepsilon_{\mathrm{v}} - \sigma_{xx} - \lambda_{xx})_t \tag{45}$$

and

$$\left(1 + \frac{\theta\Delta t}{2}\right)\Delta\sigma_{xy} = \frac{\psi}{2}\Delta\varepsilon_{xy} - \theta\Delta t(\sigma_{xy} + \lambda_{xy})_t \tag{46}$$

where Δ indicates incremental change, so that the Jacobian matrix then has the terms

$$\frac{\partial\Delta\sigma_{xx}}{\partial\Delta\varepsilon_{xx}} = K + \frac{2\psi}{3(1 + \theta\Delta t/2)} \tag{47}$$

$$\frac{\partial\Delta\sigma_{xx}}{\partial\Delta\varepsilon_{yy}} = K - \frac{\psi}{3(1 + \theta\Delta t/2)} \tag{48}$$

and

$$\frac{\partial\Delta\sigma_{xy}}{\partial\Delta\varepsilon_{xy}} = \frac{\psi}{2(1 + \theta\Delta t/2)} \tag{49}$$

Equations (24)–(31) which basically define the relationship between microcrack growth and stress intensity are programmed in subroutines which are called from UMAT. In this way, microcrack growth is factored into the stiffness matrix at each time step. A subroutine, which computes

the deviatoric stresses in each of the elements of the generalized Maxwell model (Equation (23)), is also called from UMAT. This updates the viscoelastic response for the stiffness matrix at each time step. Equations (32)–(34) define the bulk thermal changes within an element at an integration point and the subroutines which evaluate them are called from UMAT. The bulk temperature field is updated at the integration point and then passed as a boundary condition for the hot-spot model. Equations (35)–(40) encompass the development of the hot-spot model and define the occurrence of ignition. They are also called from UMAT following the bulk temperature update. Stress and strain rate values are passed from UMAT to the thermal subroutines at each time step for the work rate and friction effect calculations. As an additional comment, the Maxwell element equations and Equation (32) with the conduction term neglected, are ordinary differential equations in time. If the coefficients are assumed to be relatively constant over a time step, they may be integrated in closed form over the time step. Alternatively, a fourth-order Runge–Kutta scheme may be used or even sub-time step increments and Euler integration in time may be used. During the period of development of this model, we have used all of these methods and for the time step size required to model the transient mechanical response, we have found little difference in the results for any of them. In the results illustrated in this paper, we have used closed-form integration over the time step for both the Maxwell model and the bulk thermal model of Equation (32).

4. APPLICATIONS TO PBX 9501

The material PBX 9501 is a heterogeneous explosive consisting of 95 wt% HMX (octrahydro-1,3,5,7-tetranitro-1,3,5,7-tetrazocine) crystals embedded in a binder consisting of 50 per cent estane (a polyurethane) and 50 per cent BDNPA/F (bis (2,2-dinitropropyl) acetal/bis (2,2-dinitropropyl) formal, 50/50 wt%). The HMX crystals are bi-modal in size distribution with the formulation of 71.25 wt% Class 1 HMX (84–96 per cent smaller than 297 μm) and 23.75 wt% (75 per cent smaller than 44 μm), which is a 3 : 1 coarse/fine ratio. The explosives are pressed from molding powders and the microstructure represents an unusual challenge in engineering material modelling. This material system is selected to be used to demonstrate the applicability of the developed material model.

The viscoelastic response of PBX 9501 is herein modelled as a generalized Maxwell model having an elastic spring in parallel with four spring/dashpot elements. The values of the five shear moduli (in units of MPa) are 544.0 for the elastic spring and 173.8, 521.2, 908.5 and 687.5 for the other four springs. The values of the four corresponding relaxation times (in units of seconds) are $1.366e-4$, $1.366e-5$, $1.366e-6$ and $5.000e-7$. The value of the bulk modulus of the material is 7009.2 MPa. The assumed initial values of internal flaw size and average crack radius are 0.001 and 0.00003 m, respectively.

The first example application of the material model to PBX 9501 is a characterization of the behaviour of the crack growth portion of the model. This is done by driving that portion of the material model with uniaxial loading applied to a three-dimensional ABAQUS implicit finite element model consisting of a single element. Equations (21)–(28) define this behaviour. The assumed threshold value of stress intensity K_0 is $5.0e5\,\mathrm{Pa}\sqrt{\mathrm{m}}$, the maximum value of the growth rate of the average crack radius is assumed to be 300.0 m/s, the value of the cracking parameter to be 10, and the value of the static coefficient of friction to be 0.5. A plot of crack growth rate versus stress intensity is shown in Figure 1. The crack growth rate is seen to transition from 'slow' to 'fast' growth at the threshold value of stress intensity and begin to approach the maximum value of

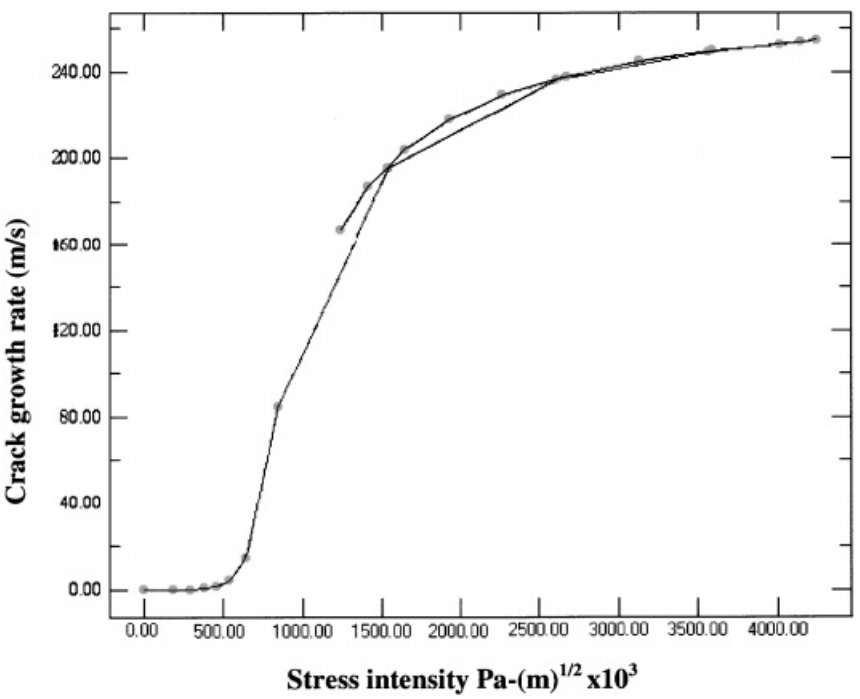

Figure 1. The crack growth rate behaviour as a function of the stress intensity for a relatively high threshold of stress intensity with transition from low crack growth to rapid crack growth illustrated.

300 m/s. At a value of stress intensity of approximately 4.3e6 Pa $\sqrt{\text{m}}$, the strength of the material peaks and unloading begins, which causes both the stress intensity and the crack growth rate to decrease.

The model would seem to be capable of well representing the brittle behaviour of PBX 9501. However, the material appears to be quite ductile at room temperature and, for this reason, a rate-dependent crack growth option must be implemented in order to simulate this behaviour. The threshold value of stress intensity is set to 500 Pa $\sqrt{\text{m}}$ and the crack growth rate is calculated as a function of effective deviatoric strain rate. The resulting simulations are compared with data collected from physical tests conducted on PBX 9501 by Gray *et al.* [21] at LANL. The comparisons are shown in Figure 2.

Additional low rate data on PBX 9501 for the interested reader are available from tests conducted by D.A. Wiegand at Picattiny Arsenal. Those data were used by Dienes to compare with his SCRAM predictions and are published in Reference [22].

In Figure 2, the peak simulated stress–strain response is seen to represent that of the material very well at both rates. The experimental curve for the higher rate is developed from reduced data obtained from a Split Hopkinson Bar test conducted at LANL, and it should be noted that the test is not being simulated. Rather, the model is instead being driven at a rate that is representative of that of the test and thus can only capture the approximate peak response. Clearly, there are some wave and bar effects in the data that are not modelled.

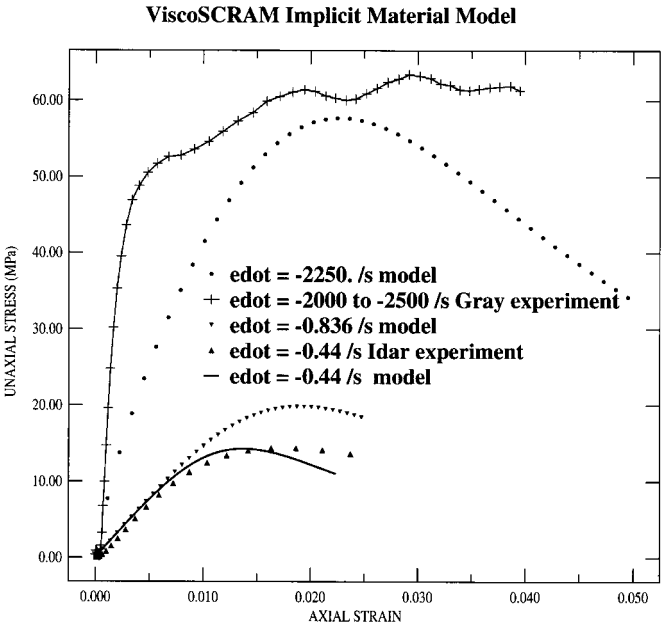

Figure 2. Simulated uniaxial stress–strain response for three strain rates with test data comparison for two of them.

The material PBX 9501 is known to have a very low value of tensile strength; the low rate tests suggest that it is about one-tenth or less of the compressive strength. Characterization of the material in tension is currently being studied at LANL and other national laboratories, but its rate dependence makes this a difficult experimental undertaking. The tensile cracking model as discussed above has been implemented, but the tensile damage growth rate is assumed to be higher in order to represent this behaviour. The uniaxial tensile response of the model for a rate of 0.44/s is shown in Figure 3, but no data are currently available for purposes of comparison.

Although no tensile data are available for comparison, there have been numerous tensile tests conducted on the material. In these tests, the peak stress and corresponding strain were recorded, unfortunately without either the test material pedigree or the test conditions (loading rate, etc.) being recorded. The model can generally predict this tensile peak stress and the corresponding strain correctly.

The third example application is the simulation of a three-point bending test. The growth of a symmetrically located damage region in an ABAQUS beam model is tracked. Tests are being conducted for the purpose of determining fracture properties of the material, and the specimen modeled has a 2 mm saw cut in the center to initiate a fracture. The model configuration is shown in Figure 4. The specimen is 75 mm long, 15 mm deep and 10 mm wide. It has been observed that a ‘damage region’ propagates from the notch vertically through the specimen at peak load, before any discrete fracture can be detected. As the centre region is damaged, the load required to continue to move the plunger downward under displacement control decreases. The details of the damage propagation, followed by discrete fracture, are still under investigation experimentally,

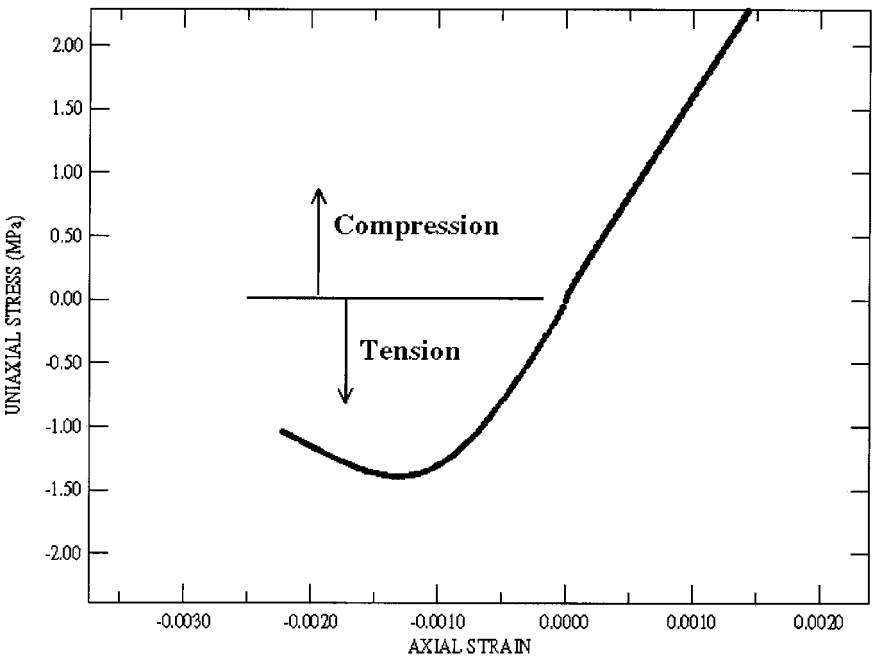

Figure 3. Simulated uniaxial stress–strain response for a strain rate of 0.44/s.

and it is not the purpose here to report them. However, the damage concept in the material model can indeed simulate this behaviour. Figure 5 shows the σ_{11} stress field along the centre region of the mesh as the peak stress is reached. As the stress redistributes because of tensile damage along the vertical plane of maximum moment ($x = l/2$), the load carrying capability of the specimen decreases. The plunger load versus the centre beam deflection is shown in Figure 6, along with one set of test data for a test conducted at room temperature with a plunger loading rate of 0.0212 mm/s.

The three-point bend simulation was carried out for the purpose of *validating* this material model, while the following example illustrates one of the purposes for which it will ultimately be used. The material PBX 9501 was developed to be a mechanically insensitive HE, that is, a mechanical insult (such as in an accident) will not normally cause it to explode. Suppose, for example, the plunger in the above calculation is thought of as a high-speed fragment from an accidental explosion impacting the beam at 200 m/s. Figure 7 illustrates the expanding wave from the impact (the plunger and supports have been removed from the graphics). Figure 8 shows a time history of the adiabatic bulk temperature increase due to the inelastic work rates and the calculated hot-spot temperatures in the centre element beneath the plunger. As the calculation continues, the temperature eventually peaks at about 12 μs and because of material failure, decreasing stresses and subsequent volumetric expansion (the only adiabatic cooling mechanism in this model), the temperature decreases slightly to an approximate steady-state value by 20 μs. The element selected to illustrate this result was not the hottest element, which actually went up to about 340 K, decreasing to about 330 K, but the result is representative. The centre element was not the hottest because the plunger contact surface is not exactly aligned with the top surface of the beam (the mesh generation tolerance

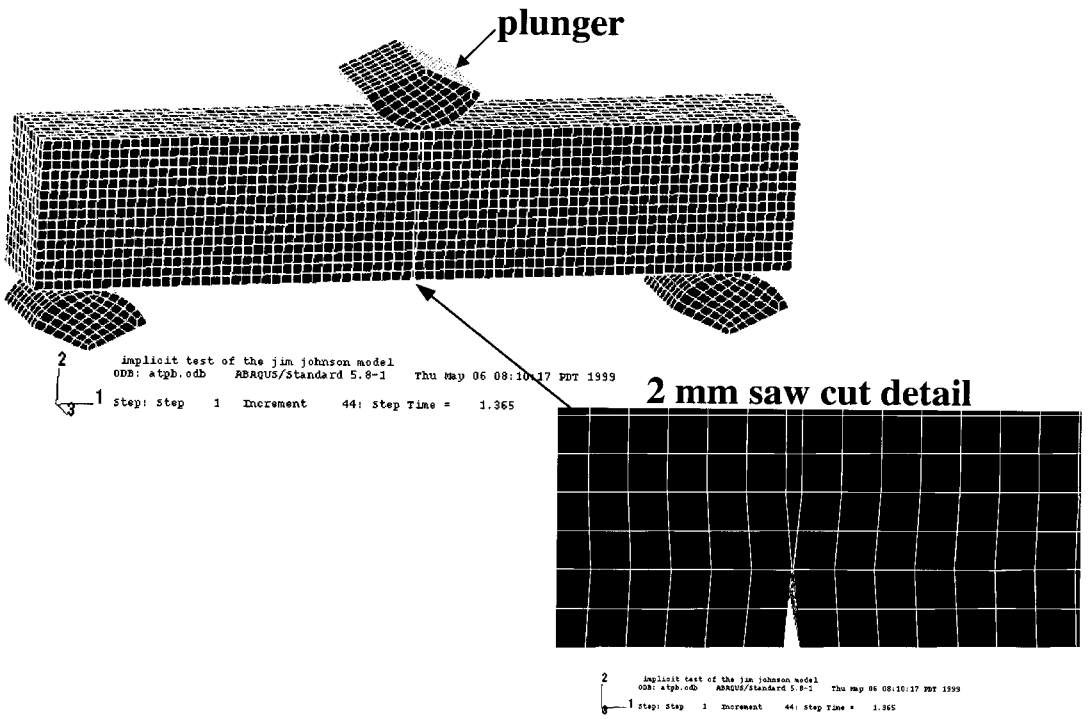

Figure 4. Three-point beam mesh configuration. The plunger was displaced downward with a velocity of 0.0212 mm/s, corresponding to the test.

was not set small enough to keep it so, and thus created what was certainly not a physically unrealistic condition!). The plunger contacts the beam slightly canted front-to-back, which makes no difference in the quasi-static simulation, but, at 200 m/s, causes a non-uniform impact.

Now, suppose that in the course of the 'accident' a fire occurred and the initial temperature at the time that the 'fragment' hits the specimen has risen to 420 K. Figure 9 shows that in the temperature contour plot at $\sim 20\,\mu$s, one element has an average temperature of 1800 K. Ignition has occurred. Figure 10 shows the temperature–time history of one integration point in this element. At $\sim 11\,\mu$s, the temperature 'runs away' as the chemical kinetics terms create ignition conditions. The runaway temperatures in this model have been limited to the gas ignition temperature of ~ 3000 K.

One further comment should be made about this set of illustrative calculations. The event simulated, might better be simulated in an explicit finite element code, as in Reference [10]. For this implicit calculation, the above result required ~ 24 h of cpu time, which is fairly long for a $\sim 20\,\mu$s simulation. On the other hand, in the quasi-static result three-point beam test validation problem above, the time (load) steps started at $1\,\mu$s and were allowed to increase to 0.05 s. A $1-\mu$s step is roughly the stable upper-limit time step for the explicit code, so that an implicit step of 0.05 s would require 50 000 steps in the explicit code, and the *multi-second* simulation result shown in Figure 6 would probably be impossible. Also, because of the rate

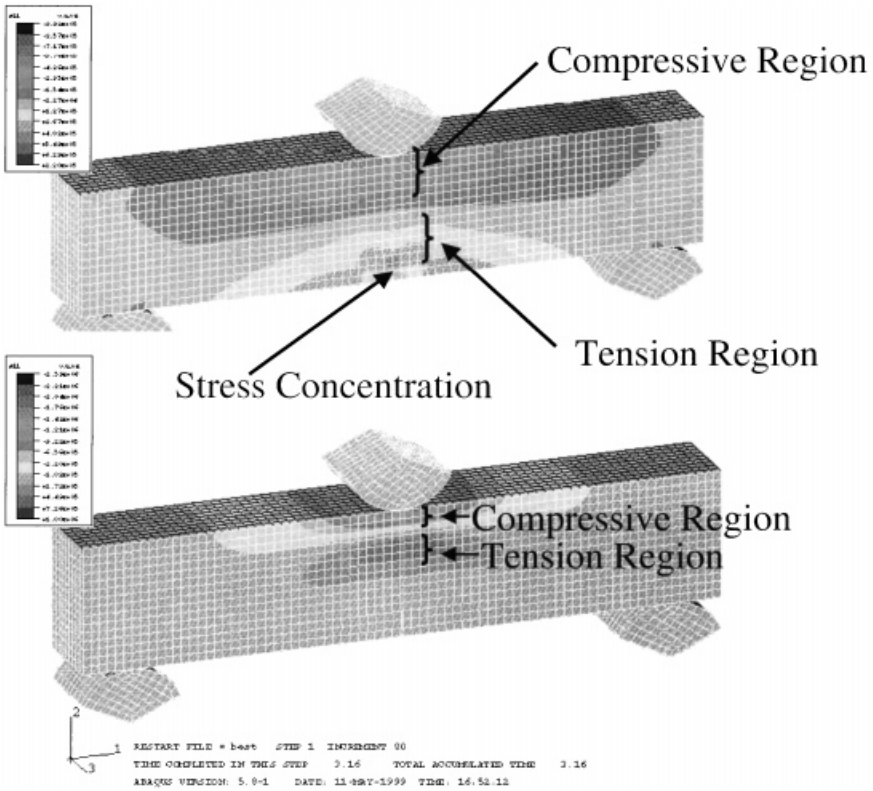

Figure 5. Two different bending stress distributions during the analysis. The top image is near the peak load, while the lower one late in the analysis shows that the only bending stress remaining in the beam (and thus the only load carrying capability) is near the plunger.

dependence of the model, it is not possible to approximate it by maintaining the loading rate at a point where the inertia effects are negligible, a common practice used to simulate quasi-static conditions with an explicit code. It might be possible to scale time in some fashion to obtain the proper rate dependence in the Maxwell model, but it is not totally clear to the authors how to handle the damage model in this fashion. The advantages of an implicit code simulation for quasi-static loading should be obvious.

5. FUTURE APPLICATIONS

The mechanically coupled cookoff (MCCO) of HE is an experiment designed to investigate the initiation behaviour of HE subject to an explosive shock at elevated temperatures (Dickson et al., 1998). In the MCCO experiment, a small flat cylinder of HE is confined radially by a one-eighth inch thick copper shell. The HE cylindrical specimen has a one-inch outer diameter and a one-eighth inch inner diameter. It is also confined on the ends by glass, ceramic or sapphire. The temperature of the HE is elevated to simulate cookoff and the inner surface of the cylinder is shocked

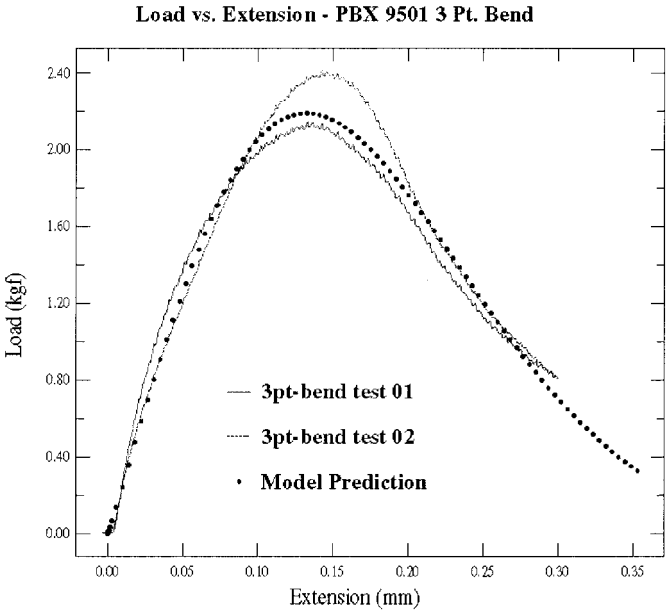

Figure 6. Load versus extensiometer data predicted by the model and measured during the three-point bend experiment on a PBX 9501 specimen containing a 2 mm saw cut on the tensile side.

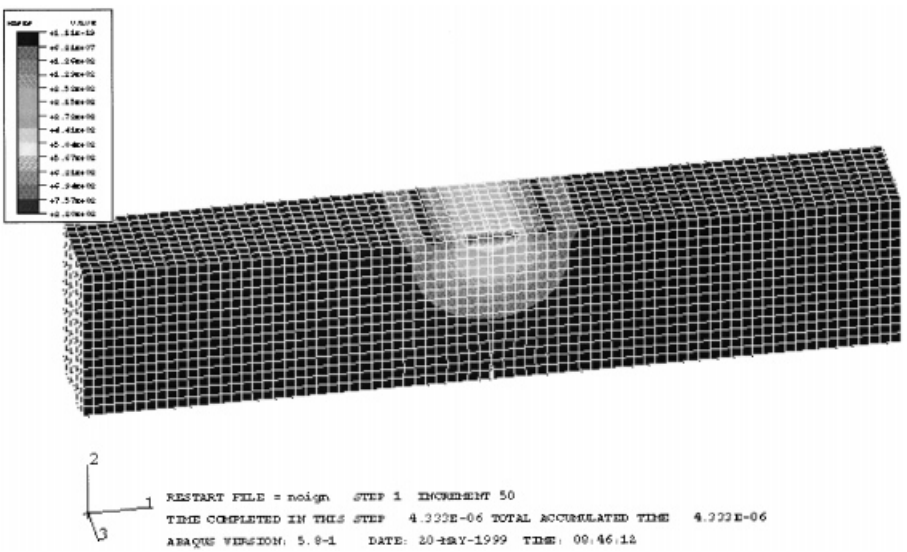

Figure 7. The Mises expanding stress wave when the plunger hits the room temperature beam at 200 m/s.

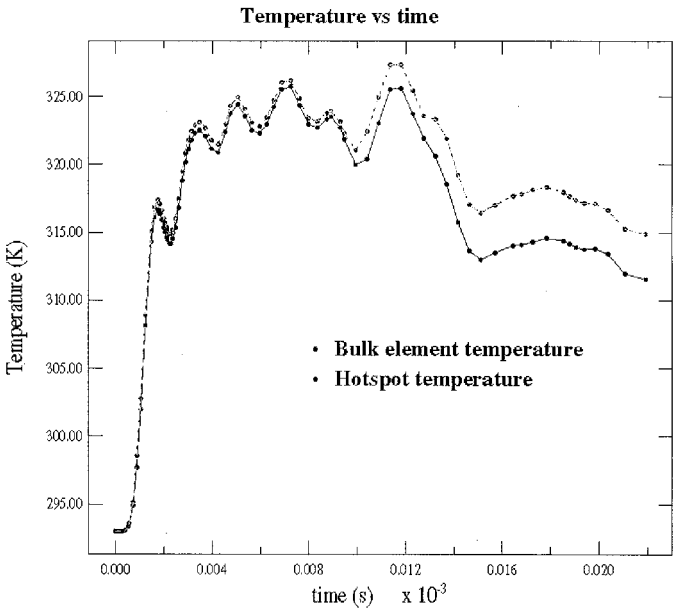

Figure 8. Temperature increase in the material under the plunger, non-ignition case.

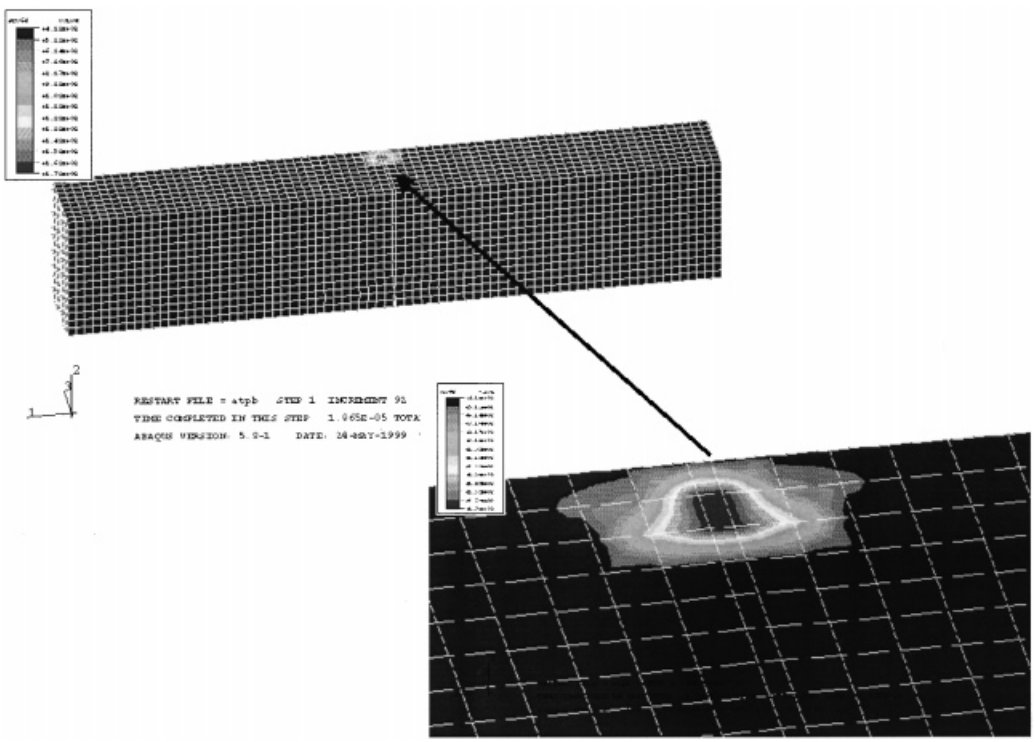

Figure 9. The 'ignition' element in the PBX 9501. The plunger and supports were removed from the graphics.

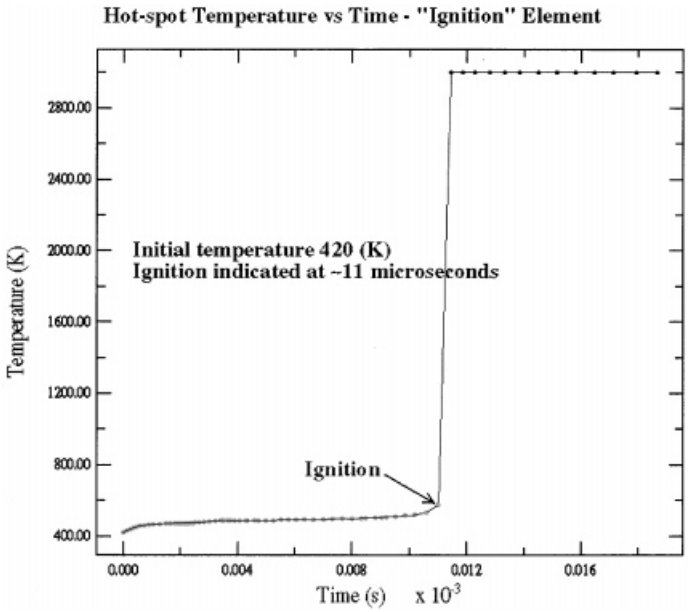

Figure 10. The temperature–time history from integration point 8 in the 'ignition element' shown in Figure 9.

with a pressure pulse created by an explosive wire. The resulting progression of events is viewed through the toughened glass or sapphire used to confine the top of the cylinder. Subsequent to the initiation of the pressure pulse, large radial cracks can be seen, along with ignition on the newly exposed surfaces of the cracks. The numerical modelling of this experiment is difficult. Many different phenomena must be incorporated into the model in order to provide the capability of accurately simulating the progression of events. The material, a particulate composite, is rate sensitive and sustains internal damage, i.e. microcracking, and the mismatches in thermal expansion capability of the composite constituents lead to a buildup of strain during the increase in temperature.

The developed material model has been implemented in an implicit ABAQUS finite element model of an MCCO experiment at LANL and plans are currently underway to perform extensive experimentation and simulation aimed at correlating model predictions with generated experimental data.

6. CONCLUSIONS

An implicit finite element material model for an energetic particulate composite material has been developed. The model simulates the interactive growth of microcracks and viscoelastic material response, complex phenomena that produce frictional forces on the sliding surfaces of microcracks that may cause localized ignition and explosion. The model has been implemented in the ABAQUS implicit finite element code and a number of example applications have been presented. The model appears to quite accurately predict material behaviour and shows promise of being a useful tool for identifying internal interacting mechanisms, phenomena that are not distinguishable through methods of physical testing.

ACKNOWLEDGEMENTS

The authors would like to thank and acknowledge several people for their contributions of experimental data and high explosive material expertise. First, Phil Howe, LANL senior project leader for high explosives, has devoted many years and much funding under his control to characterizing the mechanical, micro-mechanical and thermal behavior of PBX materials. Blaine Asay, LANL senior staff, has provided experimental results and much insight into the high strain rate mechanical and thermal response of PBX 9501, as well as funding from the Memorandum of Understanding (MOU) Program to partially support this work. Other technical staff members involved in the characterization of PBX materials at Los Alamos and their contributions to this paper are as follows: George 'Rusty' T. Gray III provided the Hopkinson Bar stress–strain results; Deanne J. Idar provided the quasi-static stress–strain data; Richard V. Browning, Richard J. Scammon, and Colin P. Sadler all collaborated to carry out the three-point bend tests and provided the results; both John K. Dienes and James N. Johnson contributed heavily to the theoretical formulation.

REFERENCES

1. Jenson RC, Blommer EJ, Brown B. An instrumented shotgun facility to study impact initiated explosive reactions. In *Proceedings of the 7th Symposium on Detonation*, Short JM (ed.). Annapolis, Maryland, 1981.
2. Green LG, James E, Lee EL, Chambers ES, Tarver CM, Westmoreland C, Weston AM, Brown B. Delayed detonation in propellants from low velocity impact. In *Proceedings of the 7th Symposium on Detonation*, Short JM (ed.). Annapolis, Maryland, 1981.
3. Dickson PM, Asay BW, Henson BF, Fugard CS. Observation of the behavior of confined PBX 9501 following a simulated cookoff ignition. *Proceedings of the 11th Symposium on Detonation*, Snowmass, Colorado, 1998.
4. Field JE, Swallowe GM, Heavens SN. Ignition mechanisms of explosives during mechanical deformation. *Proceedings of the Royal Society of London* 1982; **A 382**:231–244.
5. Field JE, Bourne NK, Palmer SJP, Walley SM. Hot-spot ignition mechanisms for explosives and propellants. *Philosophical Transactions of the Royal Society of London* 1992; **A 339**:269–283.
6. Field JE. Hot-spot ignition mechanisms for explosives. *Accounts of Chemical Research* 1992; **25**:489–496.
7. Dienes JK. Frictional hot-spots and propellant sensitivity. *Proceedings of the Material Research Symposium*, 1984; **24**:373–381.
8. Howe PM, Gibbons G Jr., Webber PE. An experimental investigation of the role of shear in initiation of detonation by impact. *Proceedings of the 8th Symposium on Detonation*, Albuquerque, New Mexico, 1985.
9. Dienes JK. A unified theory of flow, hot-spots, and fragmentation with an application to explosive sensitivity. In: *High-Pressure Shock Compression of Solids II*, Lee Davison *et al.* (eds). Springer Verlag: New York, Chapter 14, 1996; 366–398.
10. Bennett JG, Haberman KS, Johnson JN, Asay BW, Henson BF. A constitutive model for the non-shock ignition and mechanical response of high explosives. *Journal of Mechanical Physics and Solids* 1998; **46**(12):2303–2322.
11. Bazant ZP, Li YN. Cohesive crack with rate-dependent opening and viscoelasticity: I. Mathematical model and scaling. *International Journal of Fracture* 1997; **86**:247–265.
12. Li YN, Bazant ZP. Cohesive crack model with rate-dependent opening and viscoelasticity: II. Numerical algorithm, behavior and size effect. *International Journal of Fracture* 1997; **86**:267–288.
13. Addessio FL, Johnson JN. A constitutive model for the dynamic response of brittle materials. *Journal of Applied Physics* 1990; **67**(7):3275–3286.
14. Dienes JK. Strain-softening via SCRAM. *Los Alamos National Laboratory Report*. LA-UR-98-3620, 1998.
15. Dienes JK, Kershner JD. Multiple-shock initiation via statistical crack mechanics. *Proceedings of the 11th Symposium on Detonation*, Snowmass, Colorado, 1998.
16. Johnson JN. 1998; written and verbal communication.
17. Hodowany J, Ravichandran G, Rosakis AJ, Rosakis P. On the partition of plastic work into heat and stored energy in metals; Part I: experiments. *SM Report 98-7*, California Institute of Technology, 1998.
18. Frank-Kamenetskii AA. On the mathematical theory of thermal explosions. *Acta Physicochimica URSS*, 1942; XVI, **5–6**:357–361.
19. Bonnett DL, Butler PB. Hot-spot ignition of condensed phase energetic materials. *Journal of Propulsion and Power* 1996; **12**(4):680–690.
20. Hibbitt D *et al.*, *ABAQUS/Standard User's and Theory Manuals*. Version 5.8, Hibbitt, Karlsson and Sorensen, Pawtucket, RI, 1998.
21. Gray GT, Idar DJ, Blumenthal WR, Cady CM, Peterson PD. High- and low-strain rate compression properties of several energetic material composites as a function of strain rate and temperature. *Proceedings of the 11th Symposium on Detonation*, Snowmass, Colorado, 1998.
22. Dienes JK, Riley N. Strain-softening of PBX 9501. *Los Alamos National Laboratory Report*. LA-UR-98-3804, 1998.

